ADVANCED OPTICAL MATERIALS
www.advopticalmat.de

Tb and Eu in MOF-76: Elucidating the Mechanisms Responsible for the Divergent Excellent and Poor Photoluminescence Quantum Yields

Dejing Meng, Tonghan Zhao, Dmitry Busko, Arzu Cosgun Ergene, Bryce S. Richards, and Ian A. Howard**

Metal–organic frameworks (MOFs) have emerged as promising hosts for lanthanide ions owing to their ability to sensitize the lanthanides and provide a rigid topology while still permitting interactions with guest species. Among these lanthanide MOFs, MOF-76 is a noteworthy example composed of 1,3,5-benzenetricarboxylic acid (H_3BTC) and lanthanide ions. In this study, a high photoluminescence quantum yield (Φ_{PL}) of 91% for Tb-based MOF-76 (Tb-MOF) is reported, while the efficiency of Eu-based MOF-76 (Eu-MOF) is over five times lower. A potential circumvention of the poor performance of Eu^{3+} is energy transfer from Tb^{3+} to Eu^{3+}, but it is found that although energy transfer is efficient the Φ_{PL} of the Eu^{3+} remains low. The study investigates the cause of the lower quantum yield in Eu-MOF by ruling out possible factors such as crystal size, guest solvent molecules, and energy transfer from or back to the linker. None of these are significant loss mechanisms, leading to conclude that the MOF-76 ligand unfortunately leads to fast non-radiative deactivation of the Eu^{3+} excited state. The results suggest that MOF-76 is an excellent host for Tb^{3+} ions, but exploration is required for MOF linkers to simply access the potentially excellent emission efficiency of Eu^{3+} ions.

1. Introduction

Metal–organic frameworks (MOFs) belong to a class of porous and crystalline materials that are assembled from organic ligands and metal ions.[1,2] Due to their abundant and adjustable structures and properties, MOFs have been increasingly investigated as functional materials in various fields. Their potential applications include drug delivery,[3,4] catalysis,[2,5–7] sensors,[7–11] as well as gas adsorption and separation.[12–14] MOFs comprised of lanthanide ions (Ln^{3+}) and organic ligands–herein referred to as Ln-MOF–are an intriguing subclass of MOF materials with complex and diverse topologies.[2,15,16] Ln^{3+} ions possess several advantages over transition metal ions which are common to construct the MOF structure, such as higher coordination numbers, abundant coordination geometries, and unique electronic transitions resulting from the presence of 4f electrons. On the other hand, the limited absorption coefficients of Ln^{3+} ions in the UV and visible spectral region still restrict many of the potential applications of Ln^{3+} ions.[17,18] However, in the Ln-MOF structure, organic ligands can serve as sensitizers by absorbing energy and transferring it to Ln^{3+} ions, which will act as acceptors. This process is commonly referred to as the "antenna effect".[19–21] Furthermore, through the manipulation of energy transfer and integration of various emission components (including different Ln^{3+} ions), Ln-MOFs can achieve tunable emission properties, including white-light emission.[22–25] Consequently, the incorporation of Ln metals as trivalent cations in the design and synthesis of MOFs has gained considerable attention in recent years.

MOF-76 (Ln) is a highly explored Ln-MOF that is constructed using trivalent Ln^{3+} ions and benzene-1,3,5-tricarboxylate (H_3BTC) ligands with 1D channels. It has garnered significant attention due to its luminescence, stability, and porosity. Specifically, Tb^{3+} and Eu^{3+} ions are two of the most important luminescent activators, which have been regarded as attractive for usage as visible luminescent materials owing to their strong green and red emission.[26–28] Tb-based MOF-76 (Tb-MOF) was first reported by Rosi et al. in 2005.[29] In 2016, Yan and his colleagues successfully synthesized Tb- and Eu-based MOF-76 (Tb-MOF and Eu-MOF) with high photoluminescence quantum

D. Meng, T. Zhao, D. Busko, A. Cosgun Ergene, B. S. Richards, I. A. Howard
Institute of Microstructure Technology
Karlsruhe Institute of Technology
Hermann-von-Helmholtz-Platz 1, 76344 Eggenstein-Leopoldshafen, Germany
E-mail: tonghan.zhao@kit.edu; iahoward@gmail.com
T. Zhao
CAS Key Laboratory of Nanosystem and Hierarchical Fabrication
National Center for Nanoscience and Technology (NCNST)
ZhongGuanCun BeiYiTiao 11, Beijing 100190, P. R. China
B. S. Richards, I. A. Howard
Light Technology Institute
Karlsruhe Institute of Technology
Engesserstrasse 13, 76131 Karlsruhe, Germany

The ORCID identification number(s) for the author(s) of this article can be found under https://doi.org/10.1002/adom.202300867

DOI: 10.1002/adom.202300867

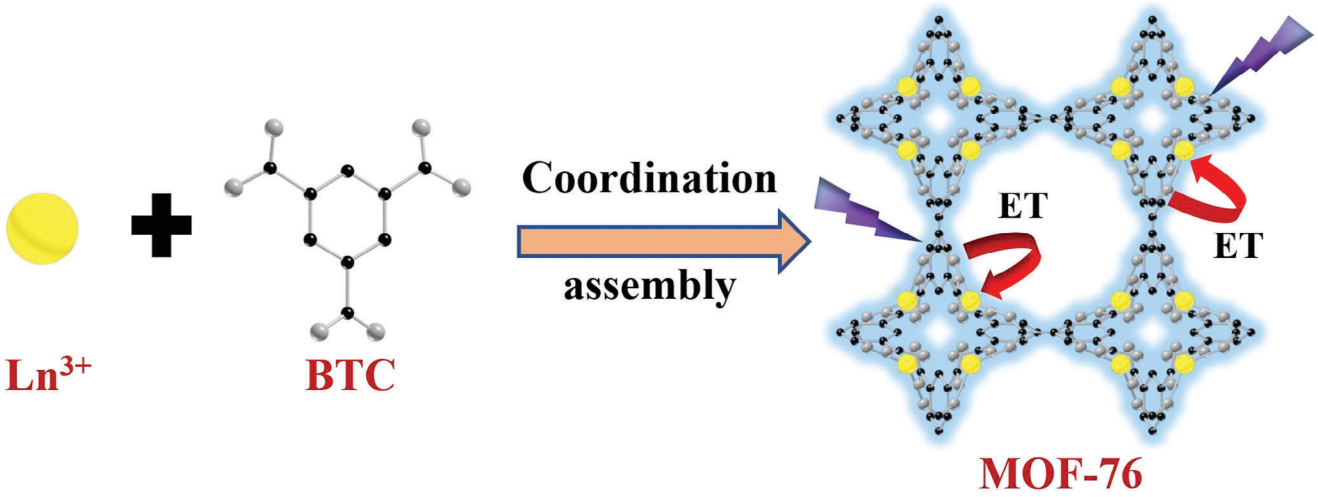

Figure 1. Diagram of synthesizing MOF-76 (Ln) structure. In Tb- or Eu-based MOF-76, upon excitation by UV light, the excited BTC could sensitize Ln^{3+} ions through energy transfer (ET), leading to efficient emission from Tb^{3+} or Eu^{3+} ions. The hydrogen atoms are omitted in the structure.

yields (Φ_{PL}) of ≈72.3% and 55.6%, respectively.[30] Microrod-shaped MOF-76 was synthesized by Yan et al. in 2017.[31] The Φ_{PL} of Eu-MOF was found to be 25.9%, while that of Tb-MOF was 58.8%. The reported Φ_{PL} of MOF-76 exhibits a significant difference between Tb^{3+} and Eu^{3+} ions as the activators despite using the same organic ligand. Among these reports, Tb-MOF possesses higher Φ_{PL} than Eu-MOF, but there is no deep research to explore the reason. Therefore, further investigations are required to understand and improve the emission efficiencies of Tb^{3+} and Eu^{3+}-based MOF-76.

In this study, we successfully synthesized Tb-MOF with a high Φ_{PL} of 91% using a microwave-assisted method that is known to deliver MOF powders in an efficient manner.[32,33] However, when we used Eu^{3+} ions as activators, the Φ_{PL} of Eu-MOF was found to be only 16% which was significantly poorer than that of Tb-MOF. We then investigated the factors affecting the Φ_{PL} of Eu-MOF, including crystal morphology, guest solvent molecules, and energy transfer between Ln^{3+} ions and BTC ligands. None of these majorly increased the Eu^{3+} quantum efficiency, leading us to suggest that the Eu^{3+} had a faster non-radiative deactivation in the MOF-76 than Tb^{3+}. This conclusion was further supported by our studies of mixed Tb^{3+}: Eu^{3+} MOFs wherein energy transfer from highly efficient Tb^{3+} to Eu^{3+} took place. We noted that in 2019 when Redel et al. fabricated heteroepitaxial Tb–Eu-BTC MOF film composing Eu-BTC on the top of Tb-BTC through a layer-by-layer approach, wherein the spatial separation of the Tb^{3+} and Eu^{3+} ions suppressed their mutual energy transfer.[34] However, here with a random distribution of Tb^{3+} and Eu^{3+} through the network we clearly observed the quenching of Tb^{3+} emission and decrease in its lifetime due to the energy transfer to Eu^{3+}. The hybrid Tb–Eu-MOF was constructed by mixing Tb^{3+} and Eu^{3+} precursors during the synthesis process. It was discovered that the emission color, intensity, and lifetime can be tuned by varying the concentration ratio to Tb^{3+} and Eu^{3+}. In an optimized situation, the Φ_{PL} of Eu^{3+} increased to 28% through the efficient energy transfer from Tb^{3+}. However, it was still far lower than that of a pure Tb-MOF. Our results prove that the BTC ligand and MOF-76 are an excellent choice for Tb^{3+}, but other hosts should be explored to enhance Eu^{3+} performance in terms of Φ_{PL}.

2. Results and Discussion

2.1. Preparation and Characterization of MOF-76 (Tb and Eu)

The formation process of MOF-76 (Ln) is schematically shown in **Figure 1**. The lanthanide precursors (salt of Tb^{3+} or Eu^{3+}) and BTC were dissolved in N, N-dimethylformamide (DMF), and deionized water (DI water) mixed solution in a microwave glass vessel. The vessel was then placed in a microwave reactor and heated to 80 °C for 2 h. Following the reaction, the products were washed with ethanol three times and dried in the air. The resulting samples were referred to as Tb-MOF and Eu-MOF, respectively. According to the previous literature, the central Ln^{3+} ions in the structure of MOF-76 were seven-coordinated by six oxygen atoms from the carboxylate groups of BTC ligands and one distorted water molecule. [35] The identical powder X-ray diffraction (PXRD) patterns (**Figure 2a**) of the as-synthesized Tb-MOF and Eu-MOF materials indicated that they were isostructural compared with the simulated pattern.[36] However, the size of the Eu-MOF crystals was markedly smaller, which was evident from the broader PXRD peaks. This was verified by scanning electronic microscopy (SEM), as shown in Figure 2b,c, which demonstrated that Tb-MOF and Eu-MOF have different morphologies and sizes. The particles of Tb-MOF exhibit rod-like and plate-like structures with a normal length of ≈10 μm. On the contrary, the particles of Eu-MOF were composed of aggregated fibers without a specific shape, and the length of isolated fibers was measured to be ≈1 μm.

2.2. Luminescence Properties of Tb-MOF and Eu-MOF

As for Figure 2d,e, the excitation spectra of Tb-MOF and Eu-MOF exhibited similar strong bands originating from BTC organic ligand absorption ≈295 nm. Based on Reinhoudt's empirical rules,

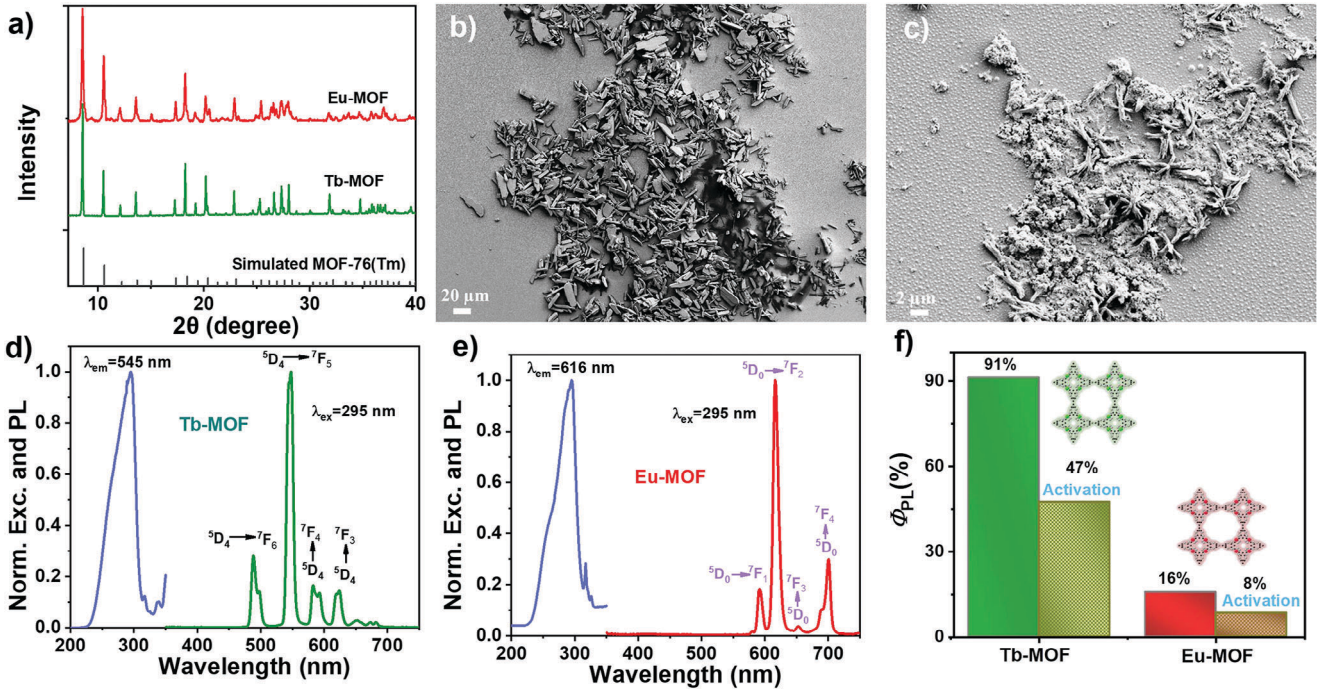

Figure 2. Characterization of Tb-MOF and Eu-MOF. a) The identical powder X-ray diffraction (PXRD) patterns of Tb-MOF and Eu-MOF. SEM images of b) Tb-MOF (scale bar: 20 μm) and c) Eu-MOF (scale bar: 2 μm). The excitation and emission spectra of d) Tb-MOF and e) Eu-MOF. f) Quantum yields (Φ_{PL}) of Tb-MOF and Eu-MOF before and after activation. Tb-MOF: excitation: 295 nm, emission: 545 nm; Eu-MOF: excitation: 295 nm, emission: 615 nm.

for efficient energy transfer, ligands should have a gap between S_1 and T_1 (ΔE_1) that is larger than 5000 cm^{-1}, and the energy of the T_1 state of the ligand should exceed the excited state of the Ln^{3+} ion (ΔE_2) by more than 3000 cm^{-1}.[37,38] We estimate the singlet energy level using the absorption spectrum of BTC (Figure S1, Supporting Information), the absorption edge is ≈297 nm indicating that BTC molecules can absorb energy to excited electrons to the S_1 state up to this wavelength. Therefore, the relative lowest absorption energy level, the S_1 state, is estimated to be at 33 670 cm^{-1}. In addition, we got the T_1 state at 25 100 cm^{-1} according to the previous published paper. We note that these are very rough estimates and coupling with the structure could affect the precise placement of these levels. In both Tb-MOF and Eu-MOF systems, the energy gap satisfies these rules (as shown in Figure S2, Supporting Information), indicating that the energy could be transferred from BTC ligands to Tb^{3+} or Eu^{3+}. It is worth noting that the BTC ligand exhibited a significantly higher triplet state energy (T_1, 25 100 cm^{-1}) compared to the emitting states of Tb^{3+} ($^5D_4$, 20 810 cm^{-1}) and Eu^{3+} ($^5D_0$, 17 830 cm^{-1}).[39,40] In that case, the ligands acted as light-harvesting chromophores and transferred the energy to Ln^{3+} ions whereas back-transfer from the Ln^{3+} ion to the ligand was expected to be negligible (this expectation is experimentally confirmed later). No emission from the ligands was observed in the Tb-MOF or the Eu-MOF as shown in Figure 2d,e. The photoluminescence spectrum of Tb-MOF exhibited the characteristic transitions of the Tb^{3+} ion at 488 ($^5D_4 \rightarrow {}^7F_6$), 545 ($^5D_4 \rightarrow {}^7F_5$), 582 ($^5D_4 \rightarrow {}^7F_4$), and 623 ($^5D_4 \rightarrow {}^7F_3$) nm. As for the Eu-MOF, the emission peaks of the Eu^{3+} ion were observed at 591, 616, 652, and 700 nm, which were ascribed to the $^5D_0 \rightarrow {}^7F_1$, $^5D_0 \rightarrow {}^7F_2$, $^5D_0 \rightarrow {}^7F_3$, and $^5D_0 \rightarrow {}^7F_4$ characteristic transitions, respectively.

Although the BTC ligands both in Tb-MOF and in Eu-MOF acted as light-harvesting chromophores and transferred energy to the Ln^{3+} ions, the quantum yields of Tb-MOF and Eu-MOF showed a significant difference, as seen in Figure 2f. Thus, the Φ_{PL} of Tb-MOF was 91%, a really high efficiency among the current reported MOF-76 materials (Table S1, Supporting Information). This excellent efficiency confirms that MOFs should be further considered as solid-state hosts for Ln^{3+} ions. At the same time, the Φ_{PL} of Eu-MOF was only 16%, which was over five-times lower than Tb-MOF. Further investigation was necessary to understand why the Φ_{PL} of Eu^{3+} was lower than Tb^{3+} and to identify potential methods to improve the Φ_{PL} of Eu^{3+}. Initially, several potential hypotheses were put forward on factors influencing the energy transfer: 1) size and morphology; 2) back energy transfer from Eu^{3+} to BTC ligand (unexpected but need to be verified); and 3) the presence of solvents in Eu-MOF leading to luminescence quenching of the Eu^{3+}.

The morphological characteristics were revealed by the SEM images (Figure 2b,c). It is commonly understood that the surface area of materials diminishes as their size and dimensions increase, leading to a marked reduction in defects.[33,41,42] Defects within the material facilitate the formation of quenching centers that promote the nonradiative recombination process and consequently reduce the luminescence. The dissimilar morphologies and sizes of Tb-MOF and Eu-MOF were attributed to variances in their respective precursors. According to previous reports, sodium acetate can function as a capping agent and

modulate the size of MOF-76.[30] In addition to the carboxylic groups of BTC ligands, Ln^{3+} ions also can coordinate with acetate groups, consequently, the competitive coordination between BTC and acetate governs the rates of nuclei formation and crystal growth. The participation of acetate groups in the reaction accelerates the formation of crystal nuclei while decelerating the rate of crystal growth, ultimately leading to a reduction in the size of MOF-76. Also, some Ln^{3+} still partially coordinated by acetate may be incorporated into the network and introduce defects.

To examine the morphology effect, Eu^{3+} precursor was changed from europium acetate to europium nitrate, and subsequently, Eu-MOF_02 was synthesized, which exhibited similar morphology to Tb-MOF as evidenced by SEM imaging and PXRD results (Figure S3, Supporting Information). Despite the much-increased crystal size, the resulting Φ_{PL} of Eu-MOF_02 was merely 18% resembling that of the sample synthesized using europium acetate. Therefore, it can be concluded that morphology-related defects were not the primary factor contributing to the low Φ_{PL}.

At room temperature, essentially no fluorescence or phosphorescence emissions of a ligand part of Eu-MOF were observed in the steady-state emission spectrum. This indicated that energy transfer from the ligand to the Ln^{3+} ion was efficient, but if there was a significant back energy transfer, we might not see it as the phosphorescence emission at room temperature could be also quite low. As to pure BTC ligands, it was easy to observe their fluorescence and phosphorescence emission at room temperature (Figure S4b, Supporting Information). There were two emission peaks around 368 and 566 nm in the steady-state spectrum. Being detected with a time-gating delayed detector mode, wherein emission was only recorded 0.1 to 10 ms after an excitation pulse, only the peak at 544 nm was observed in the spectrum, verifying the presence of the triplet level at this wavelength that was consistent with the previous report.[43] If there was back energy transfer in Eu-MOF, the energy would reach the triplet state of ligands. It would have been possible to detect the phosphorescence emissions at low temperatures due to the restriction of vibration of ligands which was beneficial to the radiative emission from the triplet state.[44–46] We measured the temperature dependence of the photoluminescence spectra and no phosphorescence of BTC was detected in the emission spectra of Eu-MOF or Tb-MOF when the temperature was varied from 98 to 293 K (Figure S4, Supporting Information). Consequently, it inferred that the low Φ_{PL} was not linked to back energy transfer (as expected based on energetic considerations).

Turning to consider the presence of coordinated solvent in MOF-76, which could influence the stronger deactivation of luminescence for Eu^{3+} ions than Tb^{3+} ions.[39] As the water molecules typically serve as quenching agents for lanthanide luminescence due to the stretching vibration of hydroxyl groups,[24,47,48] it was crucial to consider the influence of the water-containing solvent. To explore the correlation between low Φ_{PL} and solvent trapped in the MOF channels, a thermogravimetric analysis (TGA) curve was initially examined (presented in Figure S5, Supporting Information). Based on the TGA curves, Eu-MOF exhibited two thermal weight loss stages. The first stages of weight loss correspond to the evaporation of solvents located in the channels of Eu-MOF. The inflection point ≈100 °C reasonably corresponds to the boiling points of water. The evaporation of DMF was not observed, likely because DMF has been exchanged out during the ethanol washing process. The second weight loss state (≈550 °C) is attributed to the collapse of framework under high temperatures. Subsequently, based on this analysis, the Tb-MOF and Eu-MOF samples were put into a vacuum oven at 150 °C for 24 h to remove the residual solvents. However, whereas the photoluminescence spectra exhibited only a minimal variation after activation, as depicted in Figure S6 (Supporting Information), the activated MOF samples exhibited lower Φ_{PL} values. The Φ_{PL} of activated Tb-MOF reduced to 48%, while for activated Eu-MOF, the Φ_{PL} decreased down to 8% (Figure 2f). Hence, we can exclude the coordinated water as the contributing factor to the observed low Φ_{PL} of Eu-MOF. The Φ_{PL} was the best in the as-synthesized form and activation just reduced Φ_{PL}.

Based on these results, we suggested that the low Φ_{PL} observed in Eu-MOF was mainly due to a low intrinsic quantum yield ($\Phi_{Int\text{-}Eu}$) of Eu^{3+}. The $\Phi_{Int\text{-}Eu}$ can be calculated by using the measured luminescence lifetime τ and the radiative (or natural) lifetime τ_R, as given in Equation (1).[19] The τ_R, as defined, is not influenced by any factors such as energy transfer and quenching.

$$\Phi_{Int-Eu} = \frac{\tau}{\tau_R} \tag{1}$$

The radiative lifetime τ_R of Eu^{3+} can be calculated using Equation (2) via the emission spectrum of Eu-MOF.

$$\frac{1}{\tau_R} = A_{MD,0}\, n^3 \left(\frac{I_{Tot}}{I_{MD}}\right) \tag{2}$$

where, n represents the refractive index of the medium, $A_{MD,0}$ is the spontaneous emission probability for the $^5D_0 \rightarrow {}^7F_1$ transition in vacuo–where, according to previous reports, has a value of 14.65 s^{-1}–and I_{Tot}/I_{MD} is the ratio of the total area of the corrected Eu^{3+} emission spectrum to the area of the $^5D_0 \rightarrow {}^7F_1$ band.[49] Here the n was assumed to be 1.4,[50] and the calculated $\Phi_{Int\text{-}Eu}$ value was 26% which is in reasonable agreement with the measured value (especially considering the cubic dependence on the approximated n). Therefore, our findings suggest that the primary reason for the low Φ_{Eu} of Eu-MOF was likely the low intrinsic quantum yield of Eu^{3+} in the BTC framework. In the next section, we investigated whether this low intrinsic quantum yield was due to concentration quenching (i.e., transfer amongst Eu^{3+} ions until a bad site with fast nonradiative deactivation was found).

2.3. Preparation and Characterization of Hybrid Tb–Eu MOF

In order to improve the quantum yield of Eu-MOF, hybrid Tb–Eu MOF was considered due to the high Φ_{PL} of Tb-MOF. Perhaps energy transfer from Tb^{3+} to more isolated Eu^{3+} could help the Φ_{PL} of the Eu^{3+} by decreasing the energy transfer between Eu^{3+} ions and turning off the concentration quenching. A series of hybrid Tb–Eu MOF were synthesized by varying the proportion of Eu^{3+} to Tb^{3+} ions in the synthesis solution. The resulting samples were named in Tb–Eu-MOF_01 (Tb^{3+}: 95%, Eu^{3+}: 5%), Tb–Eu-MOF_02 (Tb^{3+}: 90%, Eu^{3+}: 10%) and Tb–Eu-MOF_03 (Tb^{3+}: 85%, Eu^{3+}: 15%). The accurate ratio of Tb^{3+} and Eu^{3+} ions in

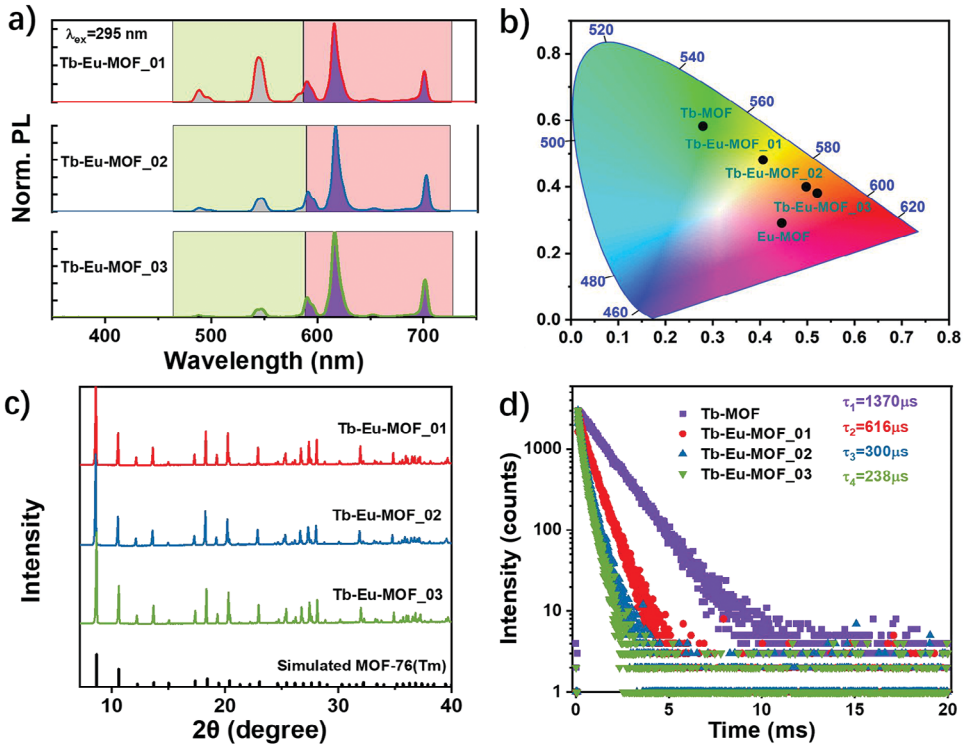

Figure 3. Characterization of hybrid Tb–Eu MOF materials. a) The normalized photoluminescence (PL) emission spectra of hybrid Tb–Eu MOF. b) The CIE image of Tb-MOF, Eu-MOF, and hybrid Tb–Eu MOF materials. c) The PXRD patterns of hybrid Tb–Eu MOF. d) Time-resolved luminescence spectra of Tb^{3+} ions monitored at 545 nm. Excitation: 295 nm, a 395 nm long pass filter was put between the sample and detector.

hybrid MOF structures can be seen in Table S2 (Supporting Information). Upon synthesis of the hybrid Tb–Eu-MOF, characteristic emission peaks of both Tb^{3+} and Eu^{3+} ions were observed in the emission spectra, as shown in **Figure 3a**. The emission peaks of Tb^{3+} ions decreased gradually with the increasing percentage of Eu^{3+} ions in the hybrid MOF, indicating possibly the energy transfer from Tb^{3+} to Eu^{3+}. In addition, the color of the hybrid MOF materials was tuned from green via yellow to orange-red at an increase in the concentration of Eu^{3+} ions in the host matrix within the MOF-76 structure (Figure 3b). As to the PXRD, the diffraction peaks of hybrid Tb–Eu-MOF were coincident with simulated MOF-76 which means these hybrid MOF were isostructural compared with the simulated pattern (Figure 3c). However, according to the morphology studies by optical microscopy (Figure S7, Supporting Information), the sizes and morphologies of the hybrid Tb–Eu MOF particles changed along with the increase of Eu^{3+} percentage. When the Eu^{3+} percentage was low (Tb–Eu-MOF_01), the morphology of the particles was similar to that of Tb-MOF. As the Eu^{3+} percentage increased to 10% in Tb–Eu-MOF_02, more rod-like particles with smaller sizes were observed. When the Eu^{3+} percentage reached 15% in Tb–Eu-MOF_03, the size of particles decreased significantly.

In terms of photophysical properties, the lifetimes of Tb^{3+} and Eu^{3+} ions were measured in hybrid Tb-Eu MOF, respectively (Figure 3d; Figure S8, Supporting Information). As shown in Figure 3d, the lifetimes of Tb^{3+} ions at 545 nm significantly decreased from 1370 to 616 μs once the Eu^{3+} ions were introduced into the hybrid structure. With an increase in the Eu^{3+} percentage to 10%, the lifetime of Tb–Eu-MOF_02 decreased further to 300 μs, and in Tb–Eu-MOF_03 (Eu^{3+}: 15%), it dropped to 238 μs. In contrast to the behavior observed for Tb^{3+} ions, the lifetimes of Eu^{3+} ions at 616 nm almost remained unchanged in the hybrid MOF structures (Figure S8, Supporting Information). As the variation in the lifetimes of Tb^{3+} was observed in the hybrid Tb–Eu MOF, thus the quenching of the Tb^{3+} emission can be attributed to the energy transfer mechanism from the Tb-centered to the Eu-centered species.[51] And below we used this to provide more information on the diffusion of excited states between Tb^{3+} ions. This energy transfer behavior was further verified by excitation spectra. For the excitation spectra of Eu-MOF and Tb–Eu-MOF_03, 700 nm was monitored because of the emission silence of Tb^{3+} ions at this wavelength. The excitation spectrum of Tb–Eu-MOF_03 shows three additional peaks at 351, 369, and 488 nm compared to Eu-MOF (Figure S9, Supporting Information). On the other hand, those three wavelengths can directly excite Tb^{3+} ions, indicating the excited Eu^{3+} ions in hybrid Tb–Eu MOF should be generated by energy transfer from Tb^{3+} ions. However, the lack of change in the lifetime of Eu^{3+} in the hybrid Tb–Eu MOF compared to the pure Eu-MOF indicates that concentration likely was not the cause of the low Φ_{Eu}.

Stern–Volmer (*S–V*) analysis is a well-known technique for studying luminescence quenching phenomena.[52,53] The *S–V* plot (**Figure 4a**) demonstrated a direct correlation between the concentration of Eu^{3+} ions and the relative lifetimes of emitters

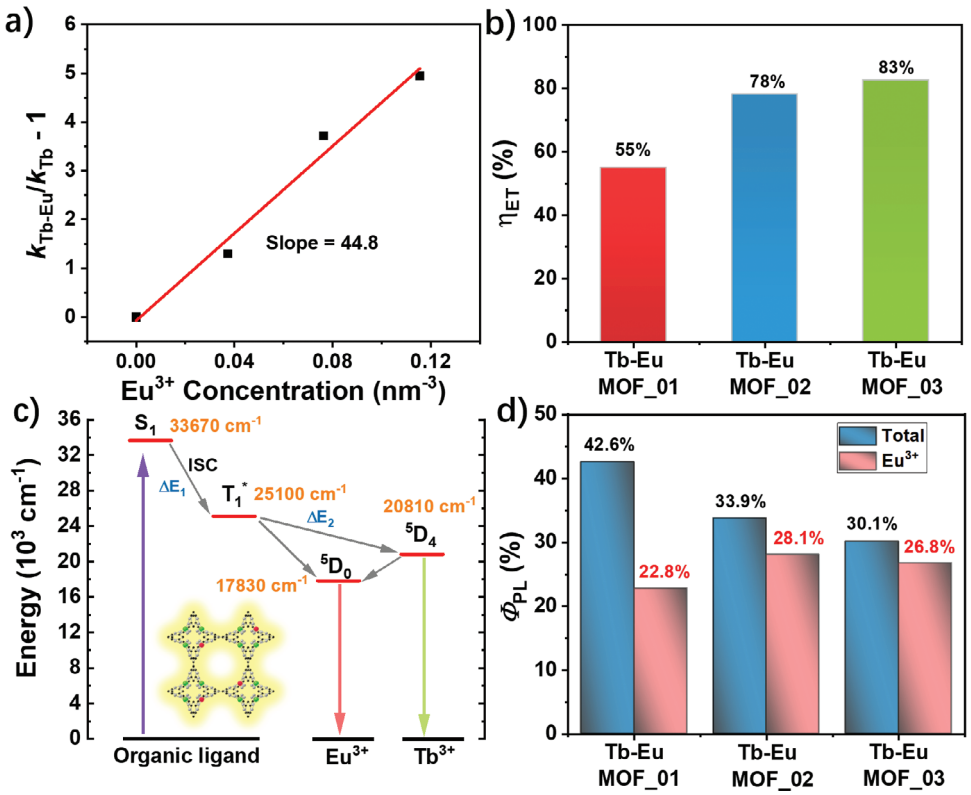

Figure 4. Investigation of energy transfer in hybrid MOFs. a) The SV plot of Tb–Eu MOF. b) The energy transfer efficiency of Tb^{3+} to Eu^{3+} ions in hybrid Tb–Eu MOF. c) The energy transfer diagram of hybrid Tb–Eu MOF. d) The quantum yields of hybrid Tb–Eu MOF.

as evidenced by the linear relationship observed. In this case, the SV equation be precisely described as:

$$K_{SV}\ [Q] = \frac{k_{Tb-Eu}}{k_{Tb}} - 1 \tag{3}$$

where K_{SV} is the *S–V* constant, $[Q]$ means the concentration of quencher (Eu^{3+}), $k = 1/\tau$, donates the transition rate, the subscripts $_{Tb-Eu}$ and $_{Tb}$ represent the hybrid Tb–Eu MOF and Tb-MOF, respectively. The linear dependence allows suggesting that the luminescent quenching was attributable to dynamic factors alone.[23] Therefore, the changes in the luminescent property of Tb^{3+} ions can be primarily attributed to energy transfer from Tb^{3+} to Eu^{3+} ions. The $K_{SV} = 44.8$ was obtained from the *S–V* plot, and the diffusion length (l_D) of the excited state of the Tb^{3+} ion was estimated by employing:

$$l_D = \sqrt{\frac{6K_{SV}}{4\pi R'}} \tag{4}$$

where *R'* is the interaction radius that was assumed to be 0.5 nm for the Tb–Eu MOF.[29] Consequently, the diffusion length of the Tb^{3+} excited state was calculated to be 6.5 nm, indicating the transfer of energy from the excited state of Tb^{3+} to Eu^{3+} could occur effectively.

As next, the efficiency of energy transfer (η_{ET}) from Tb^{3+} to Eu^{3+} can be calculated by:

$$\eta_{ET} = \frac{k_{Tb-Eu} - k_{Tb}}{k_{Tb-Eu}} \tag{5}$$

As depicted in Figure 4b, there was a gradual increase in η_{ET} at a rise of Eu^{3+} ions concentration from 55% in Tb–Eu-MOF_01 to 83% in Tb–Eu-MOF_03. In addition, we increased the percent of Eu^{3+} ions to 20% and 30% which were named Tb–Eu-MOF_04 and Tb–Eu-MOF_05, and the η_{ET} increased to 89% and 94% (Figure S10, Supporting Information). The collective energy transfer pathways within the hybrid Tb–Eu MOF are illustrated in Figure 4c. Given the high efficiency of η_{ET} between Tb^{3+} and Eu^{3+} ions, the Eu^{3+} ions in the hybrid MOF system were expected to exhibit enhanced emission efficiency. Unfortunately, the total Φ_{PL} of hybrid MOF materials (presented in Figure 4d) decreased from 43% to 34% to 30% along with the increasing percentage of Eu^{3+} ions in the hybrid MOF materials. The Φ_{PL} dropped to 20% when the Eu^{3+} ions up to 30% among the hybrid MOF structure. Therefore, too much dopant is not good at improving the total Φ_{PL}. Despite this, it was worth noting that Φ_{Eu}, as determined by calculation of the ratio of Eu-MOF emission and hybrid emission, was increasing somewhat and the maximum Φ_{Eu} was achieved in Tb–Eu-MOF_02 (28%). However, the average Φ_{Eu} remained consistent with the intrinsic value previously estimated. In addition, considering the lifetime of Eu^{3+} and the intensity ratio of $^5D_0 \rightarrow {}^7F_1$ to $^5D_0 \rightarrow {}^7F_2$ were almost unchanged, we concluded that

the intrinsic quantum yield of Eu^{3+} was still low and relatively unchanged when Eu^{3+} was diluted in Tb^{3+} MOF. Therefore, the concentration quenching to energy transfer to poor sites in the Eu-MOF was not the cause for the low Φ_{Eu}. Rather our results suggest that the low Φ_{Eu} must be due to non-radiative channels that are intrinsically present at all Eu^{3+} sites.

3. Conclusion

In conclusion, we synthesized Tb-MOF with a high Φ_{PL} more than 90% and Eu-MOF with a rather low Φ_{PL} (only 16%) based on BTC ligands. Thus, the material system was an excellent host for Tb^{3+} but a poor one for Eu^{3+}. After conducting several experiments to understand the poorer performance for Eu^{3+}, we have excluded several factors such as morphology-related surface defects, back energy transfer from Eu^{3+} to BTC ligands, and the guest quenching in Eu-MOF channels. Additionally, concentration quenching was eliminated through the inclusion of various small concentrations of Eu^{3+} in a Tb^{3+} MOF. The results therefore allowed us to conclude that the main reason for the low Φ_{PL} of Eu-MOF is the limited intrinsic quantum yield of Eu^{3+} at each Eu^{3+} site in the framework. While MOF-76 has shown to be a favorable host for Tb^{3+} ions, additional investigation is necessary to determine suitable MOF hosts for Eu^{3+} ions.

4. Experimental Section

Materials: Terbium (III) nitrate pentahydrate ($Tb(NO_3)_3{\cdot}5H_2O$) and europium (III) acetate hydrate ($Eu(OAc)_3{\cdot}H_2O$) were purchased from Sigma–Aldrich. Europium (III) nitrate hexahydrate ($Eu(NO_3)_3{\cdot}6H_2O$) and 1,3,5-benzenetricarboxylic acid (H_3BTC) were purchased from Alfa–Aesar. N, N-dimethylformamide (DMF) was purchased from Merck KGaA.

Characterization: Ln-MOF (76) was synthesized by a microwave synthesis reactor (Monowave 400). Powder X-ray diffraction patterns were obtained using a D8 Phaser diffractometer (Bruker) at 40 kV for Cu Kα with a scan speed of 10 s per step. Photoexcitation spectra were carried out on Edinburgh FS5 spectrofluorometer with an internal Xe lamp excitation source. Phosphorescence spectra and long-lived lifetime were also measured on Edinburgh FS5 spectrofluorometer using an internal microsecond flashlamp (μF lamp) as illumination source. The time-resolved decay for all samples were monitored at the characterized peaks (Tb^{3+} at 545 nm and Eu^{3+} at 616 nm with a bandwidth of 5 nm). A long pass filter was set between the sample and detector to block the scattering excitation light. Equipped with an integrating sphere (15 cm diameter, Labsphere), the absolute photoluminescence quantum yields and luminescence spectra were performed on the AvaSpec-2048×64TEC spectrometer (Avantes BV) using 300 nm UV LED (Thorlabs Inc.) as the excitation source. The thermal stage MHCS622 (Microptik BV) was used for the temperature-dependent photoluminescence measurement. Optical microscope images were captured by Keyence VH-Z500R. Thermogravimetric analysis (TGA) was carried out at a heating rate of 10 K min^{-1} under nitrogen protection on TGA/DSC 3+ (Mettler–Toledo) device. SEM images were acquired on a Zeiss SUPRA 60 VP microscope. Extinction spectra were obtained using an Agilent Cary 7000 UV–vis–NIR spectrophotometer. The ratios of Eu^{3+}:Tb^{3+} were tested by Inductively Coupled Plasma Optical Emission Spectrometer (ICP-OES).

Synthesis of Ln-MOF (76) Materials by Microwave Reactors: Ln precursors (0.28 mmol) and H_3BTC ligands (0.1 mmol) were dissolved in a mixed solution of DMF (8 mL) and deionized water (4 mL). The mixture was transferred to a glass vessel and fixed it. Then the glass vessel was placed into a microwave reactor at 80 °C with stirring 600 rpm for 2 h. After the reaction, the solid products were collected by centrifugation. Finally, the products were washed with ethanol three times and then dried in air. The dried powders were fixed between two quartz plates waiting for emission and quantum yield experiments.

Activation of Tb-MOF and Eu-MOF: The dried powder samples were stored in a glass vial and put into a vacuum oven at 150 °C for 24 h. After activation, the powders were fixed between the quartz plates for luminescence measuring.

Supporting Information

Supporting Information is available from the Wiley Online Library or from the author.

Acknowledgements

The authors gratefully acknowledge the Helmholtz Association for funding through HEMF, and the MTET program (Materials and Technologies for the Energy Transition) – Topic 1 – Photovoltaics (38.01.05), and the recruitment initiative of B.S.R. The authors acknowledge support by the KIT-Publication Fund of the Karlsruhe Institute of Technology. T.Z. gratefully acknowledges the support of the Helmholtz-OCPC postdoctoral exchange program (ZD202131) and the National Natural Science Foundation of China (22205045). Special thanks to Dr. Damien Hudry for help with the TGA measurement.

Open access funding enabled and organized by Projekt DEAL.

Conflict of Interest

The authors declare no conflict of interest.

Data Availability Statement

The data that support the findings of this study are available from the corresponding author upon reasonable request.

Keywords

energy transfer, hybrid structure, MOF-76, quantum yield

Received: April 12, 2023
Revised: September 27, 2023
Published online:

[1] N. Stock, S. Biswas, *Chem. Rev.* **2012**, *112*, 933.
[2] Y. Zhang, S. Liu, Z.-S. Zhao, Z. Wang, R. Zhang, L. Liu, Z.-B. Han, *Inorg. Chem. Front.* **2021**, *8*, 590.
[3] H. D. Lawson, S. P. Walton, C. Chan, *ACS Appl. Mater. Interfaces* **2021**, *13*, 7004.
[4] X. Zhao, S. He, B. Li, B. Liu, Y. Shi, W. Cong, F. Gao, J. Li, F. Wang, K. Liu, C. Sheng, J. Su, H.-G. Hu, *Nano Lett.* **2023**, *23*, 863.
[5] J. Lee, O. K. Farha, J. Roberts, K. A. Scheidt, S. T. Nguyen, J. T. Hupp, *Chem. Soc. Rev.* **2009**, *38*, 1450.
[6] K. Shen, X. Chen, J. Chen, Y. Li, *ACS Catal.* **2016**, *6*, 5887.
[7] D. H. Hong, H. S. Shim, J. Ha, H. R. Moon, *Bull. Korean Chem. Soc.* **2021**, *42*, 956.
[8] F.-Y. Yi, D. Chen, M.-K. Wu, L. Han, H.-L. Jiang, *ChemPlusChem* **2016**, *81*, 675.
[9] Y. Liu, X.-Y. Xie, C. Cheng, Z.-S. Shao, H.-S. Wang, *J. Mater. Chem. C* **2019**, *7*, 10743.

[10] J. M. Gonçalves, P. R. Martins, D. P. Rocha, T. A. Matias, M. S. S. Julião, R. A. A. Munoz, L. Angnes, *J. Mater. Chem. C* **2021**, *9*, 8718.
[11] H. Li, X. He, M. Zhang, X. Li, R. Wang, Z. Xu, F. Li, *Inorg. Chem.* **2021**, *60*, 2590.
[12] A. Pal, S. Chand, M. C. Das, *Inorg. Chem.* **2017**, *56*, 13991.
[13] D.-Y. Kang, J. S. Lee, *Langmuir* **2023**, *39*, 2871.
[14] X. Lu, Y. Tang, G. Yang, Y.-Y. Wang, *CrystEngComm* **2023**, *25*, 896.
[15] A. Alzamly, M. Bakiro, S. Hussein Ahmed, M. A. Alnaqbi, H. L. Nguyen, *Coord. Chem. Rev.* **2020**, *425*, 213543.
[16] T. Gorai, W. Schmitt, T. Gunnlaugsson, *Dalton Trans.* **2021**, *50*, 770.
[17] R. C. Leif, L. M. Vallarino, M. C. Becker, S. Yang, *Cytom. Part A* **2006**, *69*, 767.
[18] Y. Hasegawa, Y. Kitagawa, T. Nakanishi, *NPG Asia Mater* **2018**, *10*, 52.
[19] N. Sabbatini, M. Guardigli, J.-M. Lehn, *Coord. Chem. Rev.* **1993**, *123*, 201.
[20] M. Yuan, Q. Tang, Y. Lu, Z. Zhang, X.-H. Li, S.-M. Liu, X.-W. Sun, S.-X. Liu, *J. Chem. Educ.* **2019**, *96*, 1256.
[21] J. C. C. Santos, Y. Pramudya, M. Krstic, D.-H. Chen, B. L. Neumeier, C. Feldmann, W. Wenzel, E. Redel, *ACS Appl. Mater. Interfaces* **2020**, *12*, 52166.
[22] T.-W. Duan, B. Yan, *J. Mater. Chem. C* **2014**, *2*, 5098.
[23] Y. Yang, L. Zhao, M. Sun, P. Wei, G. Li, Y. Li, *Dyes Pigm.* **2020**, *180*, 108444.
[24] Y. Li, M. Sun, Y. Yang, H. Meng, Q. Wang, C. Li, G. Li, *J. Mater. Chem. C* **2021**, *9*, 8683.
[25] A. V. Mayeuski, D. Y. Poloneeva, E. A. Toshcheva, A. V. Bardakova, A. V. Shuruhina, A. V. Emeline, D. W. Bahnemann, *J. Lumin.* **2021**, *235*, 117970.
[26] Y. Yang, H. Huang, Y. Wang, F. Qiu, Y. Feng, X. Song, X. Tang, G. Zhang, W. Liu, *Dalton Trans.* **2018**, *47*, 13384.
[27] B. Li, W. Wang, Z. Hong, E.-S. M. El-Sayed, D. Yuan, *Chem. Commun.* **2019**, *55*, 6926.
[28] X. Mi, D. Sheng, Y.'e Yu, Y. Wang, L. Zhao, J. Lu, Y. Li, D. Li, J. Dou, J. Duan, S. Wang, *ACS Appl. Mater. Interfaces* **2019**, *11*, 7914.
[29] N. L. Rosi, J. Kim, M. Eddaoudi, B. Chen, M. O'keeffe, O. M. Yaghi, *J. Am. Chem. Soc.* **2005**, *127*, 1504.
[30] X. Lian, B. Yan, *RSC Adv.* **2016**, *6*, 11570.
[31] X. Yang, X. Lin, Y. Zhao, Y. S. Zhao, D. Yan, *Angew. Chem., Int. Ed.* **2017**, *56*, 7853.
[32] W. Yang, J. Feng, S. Song, H. Zhang, *ChemPhysChem* **2012**, *13*, 2734.
[33] S. Dang, S. Song, J. Feng, H. Zhang, *Sci. China: Chem.* **2015**, *58*, 973.
[34] D.-H. Chen, R. Haldar, B. L. Neumeier, Z.-H. Fu, C. Feldmann, C. Wöll, E. Redel, *Adv. Funct. Mater.* **2019**, *29*, 1903086.
[35] B. Chen, Y. Yang, F. Zapata, G. Lin, G. Qian, E. ? B. Lobkovsky, *Adv. Mater.* **2007**, *19*, 1693.
[36] M. Almáši, V. Zeleňák, J. Kuchár, S. Bourrelly, P. L. Llewellyn, *Colloids Surf., A* **2016**, *496*, 114.
[37] F. J. Steemers, W. Verboom, D. N. Reinhoudt, E. B. Van Der Tol, J. W. Verhoeven, *J. Am. Chem. Soc.* **1995**, *117*, 9408.
[38] H.-Q. Yin, X.-Y. Wang, X.-B. Yin, *J. Am. Chem. Soc.* **2019**, *141*, 15166.
[39] R. R. F. Fonseca, R. D. L. Gaspar, I. M. Raimundo, P. P. Luz, *J. Rare Earths* **2019**, *37*, 225.
[40] A. Y. Freidzon, I. A. Kurbatov, V. I. Vovna, *Phys. Chem. Chem. Phys.* **2018**, *20*, 16876.
[41] K. Liu, H. You, Y. Zheng, G. Jia, Y. Song, Y. Huang, M. Yang, J. Jia, N. Guo, H. Zhang, *J. Mater. Chem.* **2010**, *20*, 3272.
[42] D. Cai, H. Guo, L. Wen, C. Liu, *CrystEngComm* **2013**, *15*, 6702.
[43] X. Zhang, H. Qiu, W. Luo, K. Huang, Y. Chen, J. Zhang, B. Wang, D. Peng, Y. Wang, K. Zheng, *Adv. Sci.* **2023**, *10*, 2207004.
[44] S. Menning, M. Krämer, B. A. Coombs, F. Rominger, A. Beeby, A. Dreuw, U. H. F. Bunz, *J. Am. Chem. Soc.* **2013**, *135*, 2160.
[45] W. Zhao, Z. He, J. W. Y. Lam, Q. Peng, H. Ma, Z. Shuai, G. Bai, J. Hao, B. Z. Tang, *Chem* **2016**, *1*, 592.
[46] Y. Lei, W. Dai, Z. Liu, S. Guo, Z. Cai, J. Shi, X. Zheng, J. Zhi, B. Tong, Y. Dong, *Mater. Chem. Front.* **2019**, *3*, 284.
[47] J. Scholten, G. A. Rosser, J. Wahsner, N. Alzakhem, C. Bischof, F. Stog, A. Beeby, M. Seitz, *J. Am. Chem. Soc.* **2012**, *134*, 13915.
[48] G. E. Gomez, E. V. Brusau, A. M. Kaczmarek, C. Mellot-Draznieks, J. Sacanell, G. Rousse, R. Van Deun, C. Sanchez, G. E. Narda, G. J. A. A. Soler Illia, *Eur. J. Inorg. Chem.* **2017**, *2017*, 2321.
[49] M. H. V. Werts, R. T. F. Jukes, J. W. Verhoeven, *Phys. Chem. Chem. Phys.* **2002**, *4*, 1542.
[50] X. Chong, K.-J. Kim, P. R. Ohodnicki, E. Li, C.-H. Chang, A. X. Wang, *IEEE Sens. J.* **2015**, *15*, 5327.
[51] J. I. Deneff, L. E. S. Rohwer, K. S. Butler, B. Kaehr, D. J. Vogel, T. S. Luk, R. A. Reyes, A. A. Cruz-Cabrera, J. E. Martin, D. F. Sava Gallis, *Nat. Commun.* **2023**, *14*, 981.
[52] R. M. Melavanki, R. A. Kusanur, J. S. Kadadevaramath, M. V. Kulakarni, *J. Lumin.* **2009**, *129*, 1298.
[53] K. P. L. Kuijpers, C. Bottecchia, D. Cambié, K. Drummen, N. J. König, T. Noël, *Angew. Chem., Int. Ed.* **2018**, *57*, 11278.